AIAA JOURNAL
Vol. 49, No. 7, July 2011

Aircraft Roll Enhancement via Multi-Objective Optimization Using Surrogate Modeling

Narcis M. Ursache*
Brunel University, West London, England UB8 3PH, United Kingdom
and
Neil W. Bressloff† and Andy J. Keane‡
University of Southampton, Southampton, England SO17 1BJ, United Kingdom

DOI: 10.2514/1.J050812

This research is concerned with the design of adaptive structures for achieving global multishape morphing aerodynamic configurations by using thin-walled structures. The proposed methodologies pursue two threads toward global optimization of morphing structures, by providing means of aerodynamic enhancement using efficient structural shape optimization. A heuristic approach is proposed in this work that enables morphing through a range of stable cambered airfoils to achieve aerodynamic properties for different maneuvers, with the benefit of low-powered actuation control. This allows large changes in shape by exploiting a range of incremental nonlinear structural solutions while keeping prescribed flow improvements. Such a heuristic argument provides the basis for global shape control of three-dimensional wings and is applied to aerodynamic design to provide enhanced roll control. A hierarchical strategy is employed herein, interleaving parameterization enhancement followed by structural optimization into the aerodynamic design process, such that the design paradigm, in conjunction with global approximation techniques, is emphasized by enhanced roll while drag is minimized. This figure of merit is complemented by structural metrics and constraints to maintain product integrity.

Nomenclature

a	=	structural displacement bounds
C_D	=	drag coefficient
C_L, C_l	=	lift coefficient
C_M	=	roll moment coefficient
C_m	=	pitching moment coefficient
C_P	=	pressure coefficient
f	=	objective function
$\hat{f}$	=	approximation of objective function
f_{sec}	=	structural-related objective function
g_i	=	constraint functions
M_c	=	design cruising Mach number
n_i	=	maximum number of increments
n_p	=	maximum number of structural grid points
p, θ	=	kriging hyperparameters
R^2	=	coefficient of determination
sspan	=	wing semispan
$\mathbf{w}$	=	optimized displacement field
$\mathbf{w}^t$	=	target displacement field
$\mathbf{x}$	=	vector of design variables
Y_{CP}	=	y position of center of pressure
λ	=	kriging regularization constant
σ	=	variance of a Gaussian distribution
σ_Y	=	yield stress

I. Introduction

THE recent advances in smart materials and structures have created much interest in developing adaptive structures that can morph through different states and meet specific environment requirements or mimic nature. In real-life aircraft applications, morphing wing concepts rely on actively and continuously changing the shape of the wing to adapt it to new flight conditions, without the hinge contour discontinuity associated with conventional control/high-lift devices. Many of these technologies and applications targeting morphing aircraft [1] allow large changes in shape to maximize vehicular performance and efficiency attributes. In particular, this translates into the need for an optimum flight envelope, specific reconfiguration during different mission segments, improved maneuverability, increased survivability, optimum weight, etc. Aircraft efficiency also treats manufacturers' and operators' efforts as energy or monetary units [2] to achieve a favorable airframe configuration. This requires a design paradigm, mainly to control the aerodynamic features during the adaptation to the new environment.

Flow control represents the sine qua non of the aerodynamic morphing concept. The study of the interaction between fluid dynamics and structures has matured in the latter part of the 20th century, to provide a means of changing mission environments during flight. Such technologies can be easily claimed by pioneering polymorph planes, e.g., the tiltrotor V-22 Osprey, swing-wing F-111 Aardvark, or F-14 Tomcat. The difficulties of accommodating additional mechanisms for variable geometries and low fuel efficiency make it very difficult to achieve significant advancements in this field.

The availability of new technology and improved analytical tools, however, has opened up many new possibilities for multistructural systems. Smart aerostructures and compliant control surfaces have consequently become a potential way forward in the development of adaptive wings. Enhancements for wings are being developed to improve their efficiency in offdesign regimes. Such implementations are, apart from variable planform, related to effective camber [3] through adaptive structural concepts (also referred to as flexible, deformable, or active structures, which allow control of the geometry to adapt to the required flow) or fluidic (mainly used to control the boundary layer such that it is adapted to the geometry). The adaptive strategy resides in geometry parameters that change globally or locally to enhance flight efficiency.

Different needs have been identified in the literature to achieve morphing. Global changes are desirable by means of mechanical actuation approaches or compliant devices [4]. On a local scale, deformable surfaces can be enhanced or replaced by microsurface

Received 14 September 2010; revision received 18 February 2011; accepted for publication 20 February 2011.

*Lecturer, School of Engineering and Design. Member AIAA.
†Senior Lecturer, Computational and Engineering Design Group.
‡Professor, Computational and Engineering Design Group.

effectors (e.g., shape material alloys [5] or piezoelectric actuators [6]) or fluidic devices that adapt the boundary layer to the geometry) [7]. Such approaches offer further potential for controlling the baseline aerodynamic characteristics of airfoils. Although there has been significant research activity in the United States in the area of morphing aircraft structures, the work has been mostly directed toward military applications. Such feasibility studies have been carried out under the Smart Wing Program by Defense Advanced Research Projects Agency (DARPA), NASA, the U.S. Air Force Research Laboratory based on mechanical actuation and smart memory alloys [8], and the Active Aeroelastic Wing program to investigate the impact of aerodynamic forces on morphing surfaces for enhanced maneuverability [9], and the Morphing Aircraft Structures program funded by DARPA develops multidisciplinary technologies integrated into the aircraft structure and aerodynamics [10].

Such morphing concepts usually look at scheduling of local unidirectional geometry changes alone. Some of the morphologies are ubiquitous today (their purpose is to facilitate a wider operational envelope) and some are currently addressed in applications on contemporary aircraft in production as well as future airplane programs. But this can be further enhanced with more variability in shape change by means of combined scheduling and localized multidirectional shape change according to design intent (e.g., bistable composites [11], aeroelastic tailoring [12], passive variable winglets [13], and morphlets [14]). These exotic morphing technologies usually target the expansion of the operational envelope of future aircraft designs.

In the literature, theories based on nonlinear postcritical structural deformation to provide global wing shape control law have been proposed [3]. Such schemes provided the opportunity to derive multishape morphing control laws in order to improve upon the aerodynamic properties of morphing airfoils with the benefit of low-powered actuation control. Based on the global shape control approach of spinal structures, this paper investigates the concept of morphing wings by means of global approximation techniques in order to provide enhanced aerodynamic properties and roll control. Such analyses usually rely on sequences of parameterization, structural analysis, and aerodynamic assessment, and the large computational costs involved lead to the use of response-surface models in lieu of direct searches. The main goal of this approach is to generate enhanced wing shape adaptability that relies on a low-power actuation system [15].

II. Formulation of the Problem

An application of the proposed morphing wing methodology to transonic wing design for a narrow-body aircraft is considered here (see Fig. 1). The approach extends the two-dimensional concept of morphing airfoils by means of plates. The core of the two-dimensional case is based on stiffness tailoring of slender structures that can morph through a range of cambered shapes defining prescribed airfoils. This allows large changes in shape by exploiting a range of incremental nonlinear structural solutions under eccentric loading while meeting prescribed flow characteristics [3].

Perhaps the simplest way to envisage the current design paradigm is to consider a two-dimensional spinal structure extruded into an orthogonal direction to obtain a flat-plate model. By means of a simplistic control law, akin to the actuation scheme employed in previous methodologies addressed in the literature [3] (i.e., eccentric point forces controlling large deflections), global shape control of the new spinal structure is possible, through offset point loads at the extreme sections of the controllable outboard-wing patch.

The overall aerodynamic shape of the wing is intrinsically linked to the structural setup, and large changes in the shape of the spinal structure can have a dramatic effect on the aerodynamic performance of the wing. Here, these issues are tackled by means of constrained multi-objective optimization, with both aerodynamic- and structural-related cost functions and constraints. The geometry of the underlying spinal structure is characterized by a fixed planform and uses two patches, viz., inboard and outboard. Since the current

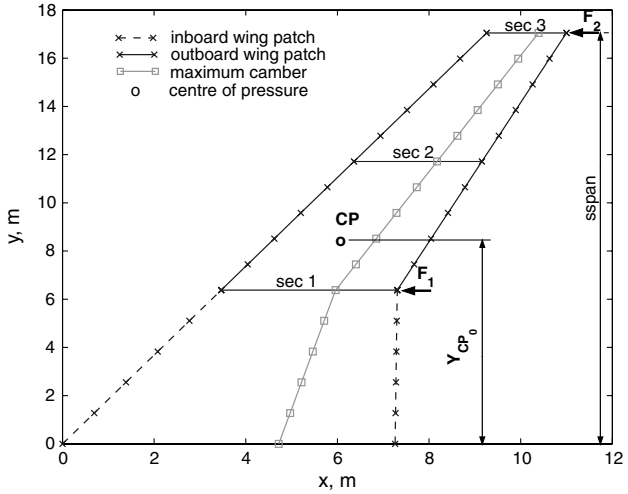

Fig. 1 Wing planform with typical inboard and outboard patches. The highlighted outboard-wing patch is actuated by point forces at the trailing edge of grid sections sec 1 and sec 3. structural-related objectives are applied to the sections sec 1, sec 2, and sec 3.

methodology makes use of a simplistic actuation law, and global shape control of the wing is needed to provide enhanced roll, the outboard-wing patch is chosen to be the active element during morphing.

The selection of the objectives in multidisciplinary analysis has a strong impact on the success of the optimization process. These are often imposed by the aircraft manufacturer such as lift, drag, weight, etc., which have a strong influence on the costs and performance of the product. Here, the main objective used defines the roll performance of the wing, while minimizing drag [see Eq. (1)]. The flow performance is highly sensitive to the smoothness of the aerodynamic shape of the wing, somewhat controlling the pressure distributions [8] and thus the overall aerodynamic performance of the wing. Such considerations lead to additional aerodynamic and structural objectives [see Eq. (2)] and constraints [see Eqs. (3–7)] to aerodynamically maintain product integrity, by enabling the morphed outboard surface to smoothly blend the controlled prescribed sections (note that the sections on which the structural-related objectives are studied here are the crank, tip, and midoutboard path positions, i.e., sec 1, sec 2, and sec 3, respectively). This translates into the use of a target wing shape, a priori generated by four-digit NACA airfoils with significant aft camber (i.e., 65% chord), to alleviate the inherent transonic flow issues over the wing and also to avoid spurious designs (to keep to the spirit of the two-dimensional approach).

As already mentioned, the underlying model is designed to enhance roll control over the wing and also to maintain the aerodynamic integrity. These two issues are tackled in a single heuristic objective f_1 by minimizing the drag gradient with respect to the position of center of pressure so that the feasible design solutions encounter low drag for a large change of center of pressure toward the tip for augmented roll.

The global load control algorithm used to solve the nonlinear problem posed breaks the simulation into a number of increments, for each of which a stable equilibrium is achieved [16]. The smoothness of the design is imposed by the objectives f_{sec} on the grid sections highlighted in Fig. 1 (i.e., sec 1, sec 2, and sec 3, corresponding to the crank, tip, and section midoutboard patch), using metrics that define the fitness of the morphed airfoils (sections) to equivalent NACA airfoils[§]; thus, the functional is defined by the L_2-norm of the difference between the deflected shape $\mathbf{w}(\mathbf{x})$ and its associated explicit target $\mathbf{w}(\mathbf{x})^t$ based on chord, magnitude, and position of

[§]Here, an implicit four-digit NACA airfoil definition is chosen due to its analytical simplicity, and the aerodynamic compromise is assumed. The design paradigm in terms of stiffness tailoring can be extended to any airfoil definition [3].

maximum deflection of deformed sections (note that this *inverse approach* works toward a given shape by attempting to push some derived characteristic toward a desired configuration). The aerodynamic constraints g_1 and g_2 are expressed with respect to the baseline-wing geometry (i.e., 2% camber spanwise, as depicted in Fig. 2); structural constraints g_3 and g_4 control the upper and lower bounds of the displacement field of the crank and tip sections; and g_5 controls the maximum yield stress criterion for the material. Therefore, the multi-objective optimization problem can be stated as follows:

$$\text{Minimize } f_1(\mathbf{x}) = \frac{\mathrm{d}\bar{C}_D}{\mathrm{d}Y_{\mathrm{cp}}} \tag{1}$$

$$f_{\mathrm{sec}}(\mathbf{x}) = \|\mathbf{w}^t - \mathbf{w}\|_2^{\mathrm{sec}} \tag{2}$$

$$\text{Subject to } g_1(\mathbf{x}) = C_{L_0} - C_L < 0 \tag{3}$$

$$g_2(\mathbf{x}) = Y_{\mathrm{cp}_0} - Y_{\mathrm{cp}} < 0 \tag{4}$$

$$g_3(\mathbf{x}) = \max|_j w_j - a_2 \le 0, \quad \text{at sec 1} \tag{5}$$

$$g_4(\mathbf{x}) = a_1 - \max|_j w_j \le 0, \quad \text{at sec 3} \tag{6}$$

$$g_5(\mathbf{x}) = \max|_{\sigma_{\mathrm{Mises}}} - \sigma_Y \le 0, \quad \mathbf{x} \in \mathbf{X}, \quad \forall\ j \in \{1, \ldots, n_p\}, \quad \forall\ \text{sec} \in \{1, 2, 3\} \tag{7}$$

with $\bar{C}_D = C_D \cdot \mathrm{sspan}$; $\mathbf{X} = \{\mathbf{x} \in \Re^n | x_k^{\min} \le x_k \le x_k^{\max}, k = 1, \ldots, n_v\}$, with $x_k^{\min}$ and $x_k^{\max}$ bounds on the n_v structural variables set by the user ($x_k^{\min} = 0.2$ mm and $x_k^{\max} = 8$ mm for control points, $x_k^{\min}|_{F_1} = -5 \times 10^3$ N, $x_k^{\min}|_{F_2} = -100 \times 10^3$ N, $x_k^{\max}|_{F_1} = 1 \times 10^3$ N, and $x_k^{\max}|_{F_2} = -1 \times 10^3$ N) (note that data are benchmarked from [3]); w_j are the deflections at the structural position j at final load increment[¶] for each of the three sections s considered defined by n_p structural grid points; and $a \in \{a_1, a_2\}$ with $a_1 = g_3(\mathbf{x})$ define the lower and upper displacement bounds for crank sections (sec 1) and tip (sec 3). The increments $\mathrm{d}\bar{C}_D = \bar{C}_D - \bar{C}_{D_0}$ and $\mathrm{d}Y_{\mathrm{cp}} = Y_{\mathrm{cp}} - Y_{\mathrm{cp}_0}$ are computed with respect to baseline geometry characteristics (i.e., $\bar{C}_{D_0} = 0.015402$, $Y_{\mathrm{cp}_0} = 7.5$ m, and $C_{L_0} = 0.51$) [17], which consist of 2% cambered grid sections spanwise (see Fig. 2). The design variables are the coordinates of the control points on nonuniform rational B-splines (NURBS) curves in order to tailor the stiffness of the structural model (see Sec. III.A). The flight case in this research is within the normal operating range for a single-aisle narrow-body aircraft, flight level FL310, a design cruising speed of $M_c = 0.78$, and Reynolds number of 7.04×10^6.

III. Wing Analysis

For the wing analysis, a hierarchical strategy is employed, interleaving parameterization enhancement by means of a CAD tool, followed by structural optimization into an aerodynamic design process, in order to study the performance of the underlying model, as shown in Fig. 3. Because of the complexity of the problem, this multidisciplinary optimization (MDO) paradigm is used in conjunction with a response-surface approximation such that design optimization is achieved, as depicted in Fig. 4. The programming challenges are augmented with the automated strategy of the MDO, since different black boxes are interdependent and provide means to study the aerodynamic and structural enhancement of such models. Each sequential work flow within the MDO is considered to be complete; therefore, it was assessed when all the numerical tools used (i.e., Abaqus for the structural analysis and VSAERO [18] for the aerodynamic analysis) reached a fully converged solution as obtained by the solvers with the built-in increments and convergence tolerances.

The aerodynamic shape design is, of course, intrinsically linked to the deformable shape of the spinal plate that satisfies the imposed design goals and constraints. The design process encapsulates the features of the underlying model by interacting both structural and aerodynamic goals, as defined in Eqs. (1–6). The main goal of the underlying MDO process is to achieve enhanced roll of the wing while minimizing the drag, designed here by minimization of the drag gradient with respect to the baseline position of the center of pressure. In the literature, a great deal of research on the optimization of aerodynamic features of wings is undertaken. The metrics used are offered mainly with respect to drag in cruise. Such criteria do not suffice for a true aerodynamic goal, and so different metrics in terms of objectives and constraints need to be involved so that enhanced properties of the optimum aircraft design are captured, e.g., buffet at high lift, pitch constraint near stall, $C_{l_{\max}}$ for clean wing, etc. (see, for instance, [19]), along with structural constraints. Intuitively, the complexity of such optimization problems is mitigated by choosing a limited number of goals and design variables and fidelity required to assess them, but runs the risk of limiting the study on the features of the aircraft.

A. Parameterization Strategy

As already noted, a myriad of feasible strategies with respect to geometry parameterization have been available in the literature since the late 1970s (see, for example, the survey provided in [20]). If combined with an optimizer, the choice of such methods becomes central to meeting the required flexibility in geometry representation through an appropriate set of design variables.

The shape parameterization technique employed in this chapter is based on NURBS surfaces definitions [21]. It has been tailored to enhance the flexibility of such surfaces and to provide a reasonable hyperspace for the design variables. Since the planform of the wing is a priori known, only the boundary shape of the outboard section is tackled, such that a full control of the displacement field is achieved during actuation. The choice of the design variables directly dictates the dependence of the kinematics of the model on the geometric NURBS patches that control the shape of the boundary, and thus stiffness tailoring is achieved via local plate-thickness variation. The design space is represented by sets of interpolating points active in the NURBS-based parameterized curves that define the bounds of the NURBS surface. Each NURBS curve is chosen to be planar, so that the defining points have two degrees of freedom only. Intuitively, a fully parameterized curve would allow the parametric space to be controlled by all degrees of freedom of defining points, but the problem would be more difficult to search within the augmented design space. In the current work, only vertical displacements of the points are taken into account, reducing the size of the parametric space. Here, the design space comprises mainly the interpolating points that define the bounding NURBS curves, i.e., six points for each parameterized section (i.e., crank and tip) and five points in the orthogonal direction. This scheme of points is chosen to keep to the spirit of the two-dimensional approach and also to allow a large variation of the curvature of the surface, which intrinsically dictates the thickness distribution of the platelike outboard wing. A random set of variables during the optimization process leads to the variation of the surface based on interpolating points of the NURBS in crank, leading edge, and tip positions is shown in Fig. 5.

The NURBS surface is constructed based on quadrilateral patches, such that the geometry of the outboard wing is fully captured, as shown in Fig. 5. The structure of the patches (i.e., the control net) is fully defined by control and/or interpolating points of the bounding NURBS. This allows the surface to be discretized evenly in the geometric space by creating a set of internal nodes, such that an isoparametric mapping of the discretized surface onto the finite element space is possible. This equidistant mapping in the parametric design space augments the finite element discretization properties, by exporting the internal node set and also the nodal thickness to create a shell structure using a standard format, viz., IGES (Initial Graphics Exchange Specification [22]).

[¶]Because of high computational expense, only the final increment from the nonlinear solver is analyzed (as opposed to the analysis of multicambered morphing state airfoils from [3]) and is set by a stopping criterion, i.e., $a_1 = \mathbf{max}|_j w_j$ at sec 1.

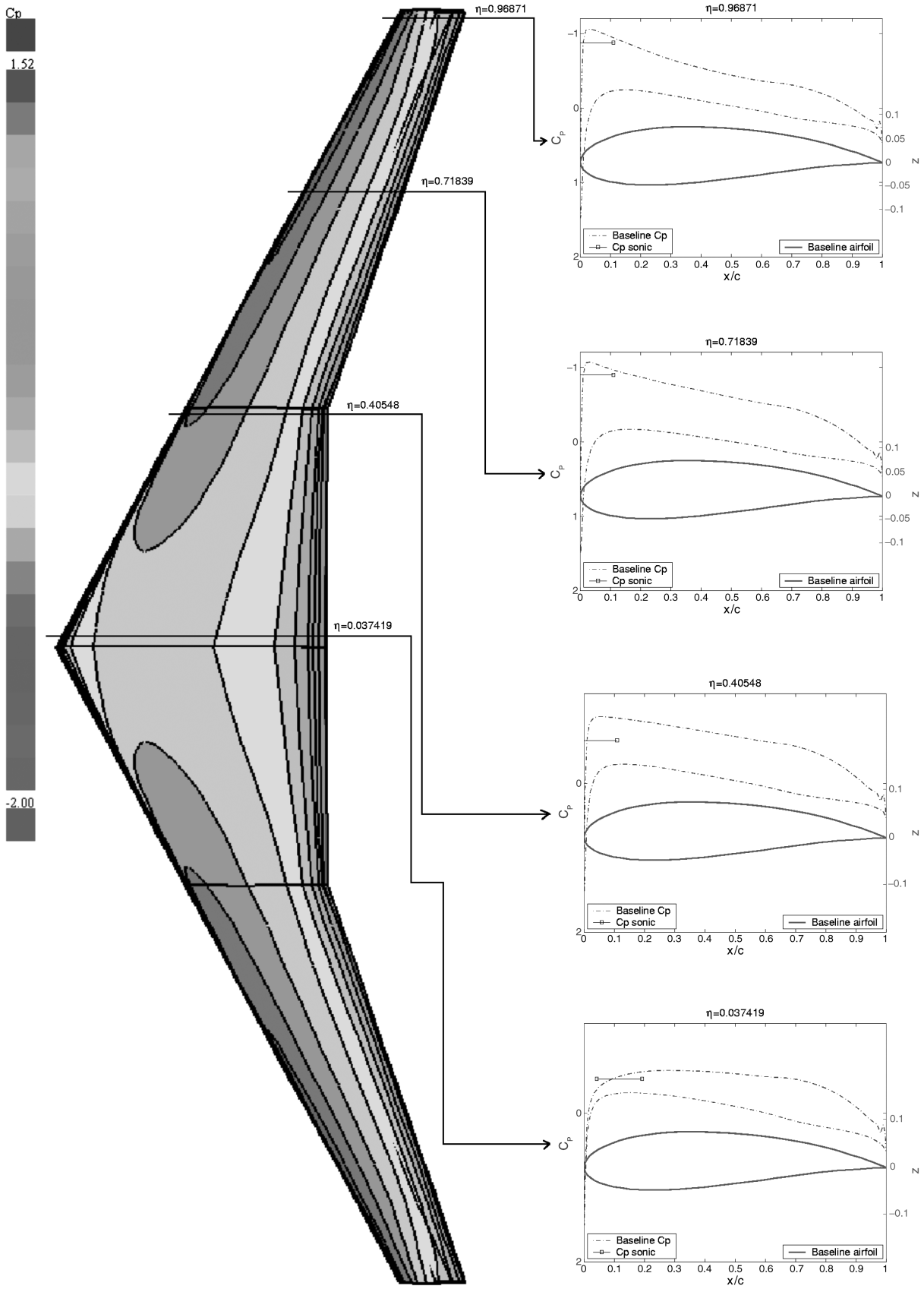

Fig. 2 Pressure contours of the baseline wing.

B. Finite Element Formulation

Tracing smooth equilibrium paths of a loaded structure that encounters critical points becomes impossible for classic load or displacement control techniques [23], as the perturbation parameter should follow the nonlinear path in a constant gradual manner. The solution becomes in this case nonunique in the hyperspace with snap-through or snap-back behavior. To capture the instabilities, such methods can be enhanced by the *arc length* method, initially introduced by [24], in conjunction with an incremental numerical Newton–Raphson algorithm. A multidimensional control parameter

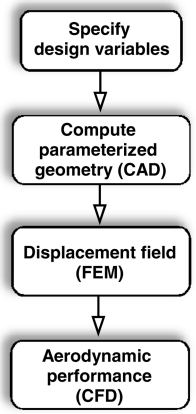

Fig. 3 Sequential wing workflow.

technique, within the field of perturbation theory, is approached by [25], with the benefit of reducing the dimensionality of the problem to a single parameter approach. First and second path derivatives, based on a Taylor expansion consistent to Koiter's theory [26] are used to set the subsequent equilibrium path, which is in contrast to classic methodology.

A considerable amount of work has been done in the field of structural optimization of frames and plate structures. Primarily, these are designed with respect to state variables to enhance buckling resistance (see the comprehensive review of [27]). As an alternative to numerical approaches to solve complex structures, closed-form solutions of plates under different schemes of discretization are also offered in the literature, with the aim of achieving global closed-form solution of the continuum model. The analysis context of such models is to capture static or dynamic behavior, in a combination of wide analytical element definitions (specifically, for thin- or thick-plate assumptions).

Within plate theory, one can classify the existing methods according to the deformation assumptions used: namely, classical plate theory, first-order shear deformation theory, or high-order shear deformation theory. For the purpose of buckling calculation, classical plate theory is valid for thin shells and, based on equations from [28] (for moderate rotations), based on Love–Kirchhoff hypothesis: that is, a normal to the plane middle surface remains normal and straight after deformation. This hypothesis is weakened by high transverse shear strain; therefore, the baseline model is prone to transverse failure [29]. This drawback is overcome with first-order shear deformation theory, which uses the Reissner–Mindlin hypothesis, where the normal is allowed to rotate relative to the reference surface [30]. A general approach to thick and anisotropic plates, but more computationally expensive, is high-order shear deformation theory, as this requires computation of high-order strains.

These theories are readily accounted for within Abaqus, the commercial finite element tool used in this work by means of a wide library of elements consisting of general-purpose thin- and thick-shell elements. Here, the parameterized outboard wing spans 10 m and has a maximum thickness of 15 mm, so it would be considered to be a thin shell, under the Love–Kirchhoff hypothesis (the thickness-to-span ratio is less than 1/15). Abaqus imposes such hypotheses numerically on the shell definition, where the transverse shear stiffness K_γ is treated as a penalty [31]:

$$K_\gamma = \frac{G_\gamma t \Delta \mathcal{A}}{1 + (q \Delta \mathcal{A}/t^2)} \tag{8}$$

where G_γ is the elastic moduli, t is the thickness of the shell, q is a relaxation factor, and $\Delta\mathcal{A}$ is the area of the reference surface [31].

The element type chosen for this type of analysis is a quadrilateral small-strain thin-shell element S4R5 (i.e., four nodes, reduced integration with five degrees of freedom per node), suitable to capture nonlinearities where the surface and the displacement field are assumed to be smooth, but with a tradeoff in accuracy [32]. These shear flexible small-strain shell elements are computationally more relaxed, since they account for five degrees of freedom per node, as the normal to the surface (the metric from which most variables are derived) is defined by only two independent variables (i.e., two

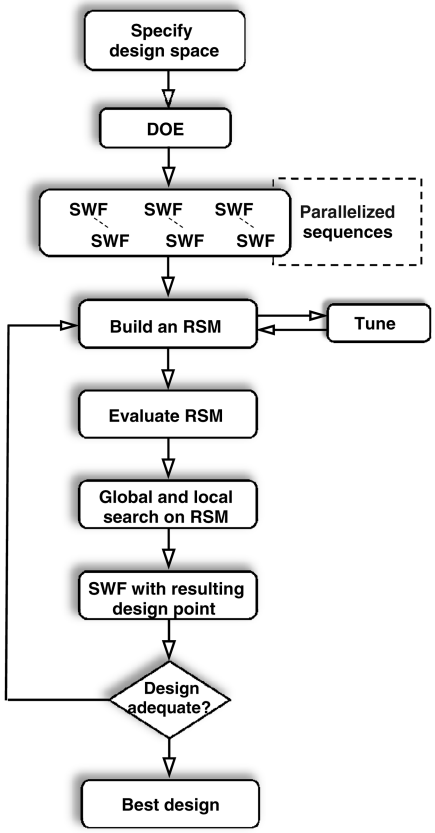

Fig. 4 Optimization strategy.

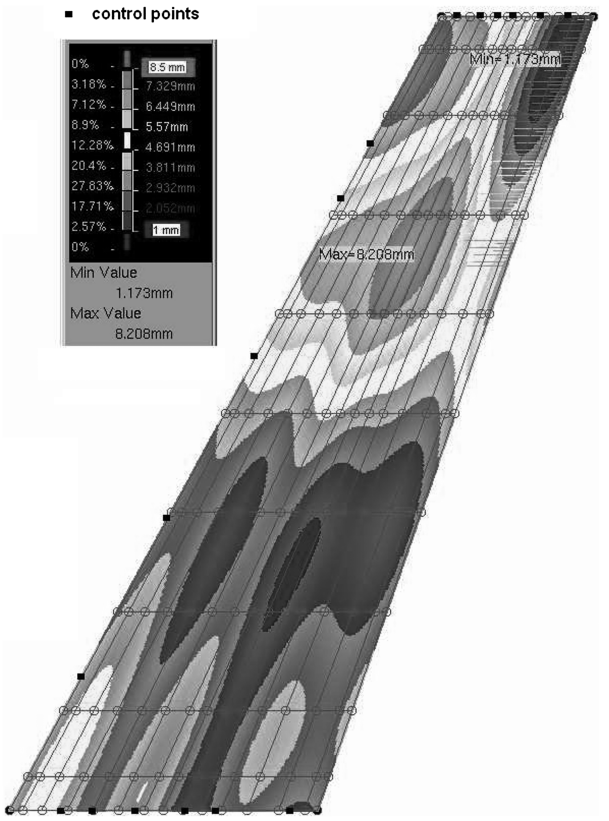

Fig. 5 Outboard NURBS parameterization and a random thickness distribution of the plate during the optimization process.

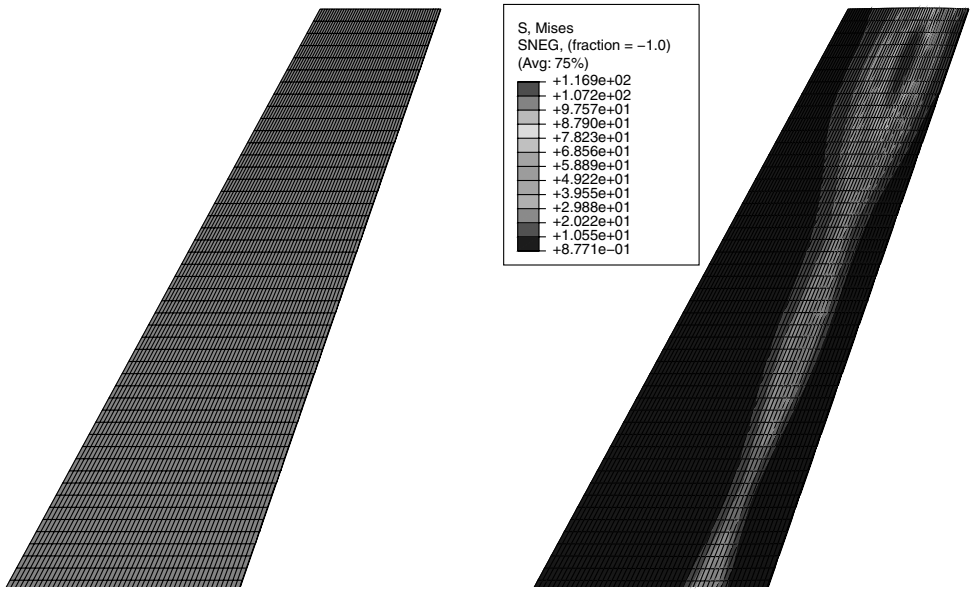

a) Outboard structured mesh **b) Stress state, MPa**

Fig. 6 Outboard finite element discretization and the corresponding stress state of the randomly parameterized outboard patch from Fig. 5.

arbitrary initial orthogonal directions) [31]. Further, the points on the surface and the component vectors of the normal to the surface are interpolated separately.

Mapping equally spaced points from the CAD tool onto the finite element boundaries, a detailed finite element analysis structural discretization and the corresponding stress state of the randomly parameterized outboard patch from Fig. 5 are shown in Fig. 6. Clearly, larger displacements can occur in the area of interest, i.e., the tip of the wing, if the bending stiffness is tailored to provide more flexibility locally and enhances the stress state due to the camber cusp on the aft-camber driven profile, as depicted in Fig. 5. The numerical model consists of 3000 shell elements and 121 solid elements used to model the eccentricity, as shown in Fig. 7 (note that the eccentricity is modeled with solid elements to accurately transmit the load and resulting torque spanwise to the shell). A shell-to-solid coupling is used here to provide continuity to the stress state and displacement field. The model consists of 19,642 degrees of freedom, which needs a significant amount of CPU time and computational capacity, making the cost of the analysis quite high. The run time is also augmented by the high degree of nonlinearity encountered by the model (this is mainly dictated by the constitutive kinematics definition). Such issues, for this particular analysis, make Abaqus a limiting factor in the performance of the MDO, even if the process is parallelized. Therefore, a careful manipulation of input/output data is needed to avoid bottlenecks on disk and memory issues.

C. Computational Fluid Dynamics Analysis

The aerodynamic characteristics of the morphing wing are provided here by VSAERO [18], a panel or boundary element method that solves the linearized potential equations for inviscid, irrotational incompressible flow, with additional compressibility correction (i.e., Prandtl–Glauert and Kármán–Tsien rules). The method is enhanced for boundary-layer calculations, provided by a viscous-potential flow coupling. The advantage of using VSAERO is that only a surface discretization is necessary, since it based on a classical panel method, and does not require a grid in the flowfield. The method is limited to certain flows that include relatively high Reynolds numbers and small angles of attack, applied to slim bodies with closed surfaces, up to low transonic speeds.

A typical VSAERO model of the wing surface and wake panels is shown in Fig. 8. The generating airfoils are based on cosine spaced grid coordinates, to provide closely spaced panels at the leading and trailing edges of the wing. The streamwise wake panels are chosen to provide a fine mesh downstream of the wing tip, after which their density decreases following a cosine rule.

The choice of the design variables in an optimization problem becomes particularly important using aerodynamic elements related to the performance of the aircraft. These elements are inherently linked to drag, which, becomes the direct measure here of aerodynamic performance. Several methodologies proposed in the field of concept design deal with optimizations based on performance assumptions, including sections, planform, etc., and are usually associated with a large design space and low-fidelity analyses. The detailed design, consisting of smaller design space but higher-fidelity analyses, limits the improvement over the design during optimization, but may converge more quickly to a feasible solution. Therefore, the selection of airfoils with a priori known performance is crucial. Since the present approach is studied in transonic conditions, an extreme-aft-camber NACA airfoil is chosen to define the wing spanwise.

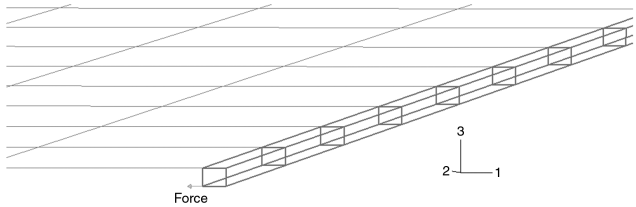

Fig. 7 Shell-to-solid eccentricity coupling.

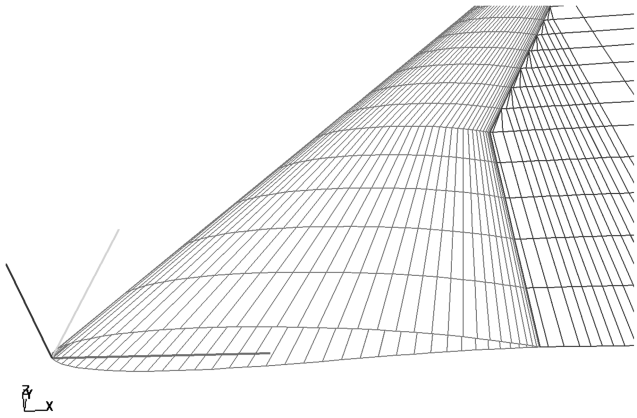

Fig. 8 Common boundary-fitted aerodynamic grid for wings.

IV. Kriging and Model Verification

As already mentioned, the MDO paradigm is based on response-surface approximation, following the strategy in Fig. 4. The quality of the response surface depends upon the values of the true function evaluated at sample points within the domain, often defined as *hypercube*, generated by design-of-experiments (DOE) algorithms [33]. The design optimization process is carried out on the surface approximation to meet the cost functional required. The strategy also involves an update process, where feasible solutions found on the fitted response-surface methodology (RSM) to the initial data may be fed back to the training pool for further updates and surface refinement. This process is repeated until some form of convergence is met. There are a number of techniques of DOE available in the literature that seek to sample the entire design space to capture most of the landscape of the function [17]. Here, an $LP\tau$ DOE array is used for its space-filling characteristics and capability of updating the training pool without the repositioning the already-evaluated design arrays and running the risk of clustering the data sets.

Based on an $LP\tau$ array, the kriging definition is employed [17] here, due to its ability to capture complex functions and provide error estimates in order to provide means of global approximation of the underlying model (note that the kriging methodology is applied for each of the objectives and also for aerodynamics-related constraints). Two forms of kriging are employed in this study to provide a parallel on cost-effective approaches and are referred to as full kriging (i.e., the hyperparameters θ and p are assigned to each variable),

$$\mathbf{R}(\mathbf{x}_i, \mathbf{x}_j) = \exp\left[-\sum_{j=1}^{k} 10^{\theta_j}(\|\mathbf{x}_{n+1,j} - \mathbf{x}_{i,j}\|^{p_j})\right] + 10^{\lambda}\delta_{ij} \quad (9)$$

and a reduced form of kriging (i.e., the hyperparameters are assigned to groups of variables),

$$\mathbf{R}(\mathbf{x}_i, \mathbf{x}_j) = \exp\left[-10^{\theta}\sum_{j=1}^{k}(\|\mathbf{x}_{n+1,j} - \mathbf{x}_{i,j}\|^{p})\right] + 10^{\lambda}\delta_{ij} \quad (10)$$

where the hyperparameter p_j can be thought of as determining the smoothness of the approximation function, and θ_j can be thought as of determining the impact on the approximation function with changes of $\mathbf{x}_{n+1,j}$ with respect to $\mathbf{x}_{i,j}$.

The initial stage of the workflow from Fig. 4 is based on computing an initial set of experiments, after which an approximation surface is fitted to the data. This kriging is then tuned with respect to the hyperparameters to maximize the likelihood function in a two-stage search, i.e., genetic algorithm (GA) [34] for 3000 steps with a population of 100 and then a further 2000 steps in a dynamic hill-climbing (DHC) search [35] to locate maxima in an invariably highly multimodal problem. Here, the initial LPτ array comprises 200 design points directly evaluated within the sequential workflow (SWF) presented in Fig. 3 and is augmented by another 155 design points used for prediction that provide a means to assess the quality of the response surface. This work flow is computed for each of the objectives [i.e., aerodynamics-related f_1 and structural-related f_{sec} from Eqs. (1) and (2), respectively], and aerodynamics-related constraints [i.e., g_1 and g_2 from Eqs. (3) and (4), respectively]. The design space comprises 17 parameterization points, in addition to two point forces, which translates into an approximation parametric space with 39 hyperparameters for the full-kriging definition and only three hyperparameters for the reduced-kriging definition.

Based on the approximation surfaces built for each objective and the aerodynamics-related constraints, a quality check of the RSMs is possible. This procedure is enhanced when using a set of prediction points already evaluated within the SWF, which are then compared with the predicted values by the RSMs at the specified locations of the prediction points. Consequently, the quality of the RSMs is based on the linear regression between the current data (i.e., prediction points) and the predicted values by the RSMs, as depicted in Fig. 9a for the full kriging and in Fig. 9b for the reduced kriging (note that all functionals have been processed, but only the edifying ones are presented here for analysis purposes).

To encapsulate a broad range of aspects of the underlying model, both numerical and graphical measures of the fitness of the entire data set are employed here. When using numerical methods, a measure of the goodness-of-fit statistics may mislead the true features of such large metamodels, by compressing some aspects of the data into a single predictor, such as the factor of determination R^2 or standard root-mean-squared error (rmse) [36]. Graphical methods have the advantage over numerical methods by encapsulating more features of the candidate model, e.g., change in spread of the residuals, leading to various assumptions on standard deviation and methods to validate the fitness.

Graphical methods are employed here by means of residuals plots, initially based on the assumption of constant standard deviation across the data. The method employed for such assumption is an ordinary least-squares (OLS) regression to determine the parameter estimates [37,38]. A potential pitfall of using OLS is that the variation trend exhibited by the residuals might not model the deterministic part of the data accurately, leading to a changing variance across the model. In such cases, the residuals will not follow an evenly spread trend, but will emphasize the presence of the *outliers*, which can bias the prediction and alter the parameter estimates. Therefore, a weighted procedure is also employed by means of iteratively reweighted least-squares (IRLS) [39] on the assumption of non-constant standard deviation. The outliers reside in inconsistencies with the bulk data and can dominate the regression (although, if

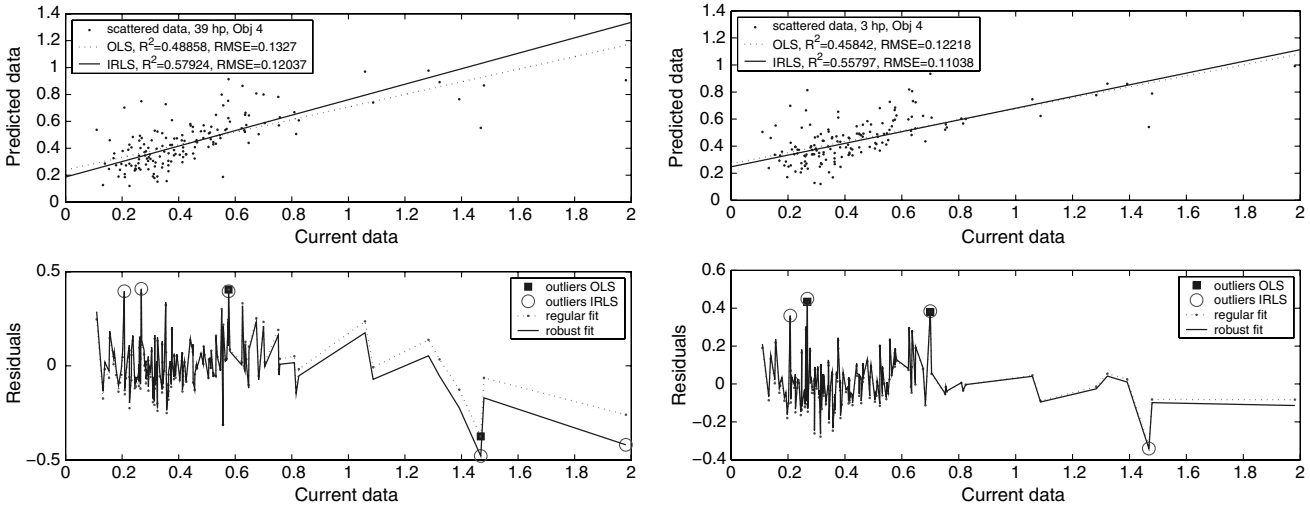

a) Objective f_{sec3} **b) Objective f_{sec3}**

Fig. 9 Objectives and constraints: goodness-of-fit statistics, full kriging (39 hyperparameters), and reduced kriging (three hyperparameters).

dropped, can increase the correlation between the independent and dependent variables), but the outliers may also contain engineering interpretation about the data under investigation and therefore, ideally, should not be removed. The source of the outliers might be partly converged solutions (i.e., structural or aerodynamic in nature) and can be repaired by making use of high-fidelity analysis tools (see, for instance, [40]). The negative impact of the outliers on the regression plane can be alleviated by using the IRLS method, as it assigns different levels of quality to data through quantitative means of *weights* to control the contribution of each observation to the parameter estimates. The advantage of using IRLS over a number of hybrids of OLS (e.g., IRLS with Huber weighting technique, univariate outlier, and multivariate outlier removal) is also emphasized by [41] in a neuroimaging study on hemodynamic shapes, achieving robust parameter estimates with artificial influential outliers, iteratively down-weighted on the principles of [37] (i.e., the residuals are standardized with respect to the median absolute deviation technique that is also used in the current work).

By means of numerical measures, the figures of merit are represented here by R^2 and rmse. The coefficient of determination R^2 measures the variability of the prediction with the independent variable and is a nondimensional figure with higher values, usually leading to a better correlation of the responses. Often, however, larger correlations also occur due to data dependency, leading to residual autocorrelation, and do not guarantee that the model fits the data as expected [38]; further, they cannot explain the underlying model. The correlation factor is defined as

$$R^2 = \frac{S_{f\hat{f}}}{S_f S_{\hat{f}}} = \left(\frac{n\sum f_i \hat{f}_i - \sum f_i \sum \hat{f}_i}{\sqrt{n\sum f_i^2 - \left(\sum f_i\right)^2}\sqrt{n\sum \hat{f}_i^{\,2} - \left(\sum \hat{f}_i\right)^2}} \right)^2 \tag{11}$$

where S_f is the covariance between independent variable f and the approximate function $\hat{f}$, and n is the number of data points for regression.

To mitigate any false fitness, an additional statistical component is used here: namely, rmse, which is exhibited by the underlying model, and values closer to zero indicate a better fit:

$$\text{rmse} = \sqrt{\frac{\sum w_i (f_i - \hat{f}_i)}{n-2}} \tag{12}$$

where w_i are the weights associated to the residuals.

The scatter in the residuals shown in Fig. 9 adequately describes the systematic variation in the data, with a nearly even spread trend, apart from the regions where outliers occur. The scatter also outlines the validity of the initial error assumption of constant variance across the data in most of the cases, which would allow the OLS to perform well. But this would not suffice in drawing a silver-bullet conclusion on the fitness of the model, and the IRLS technique is also performed in conjunction with the outliers present in the data (note that a number of outliers are expected in the data trends, due to the underlying multipoint design model). The IRLS is used to alleviate the false significance of some parameter estimates under influential outliers. Clearly, the IRLS is more flexible in accommodating levels of quality to the responses on the assumption of nonconstant variance and is also resistant to the influence of the outliers,** so that better correlations and standard errors are achieved. Optimizing the weight vector to find the parameter estimates allows IRLS some improvement on the quality of the model, more noticeable in cases with multiple outliers that can heavily alter the regression plane computed with OLS (see Fig. 9). rmse also augments the improvement and goodness of fit, encountering diminished values.

**Herein, the outliers have been computed using both OLS and IRLS techniques on the standardized cross-validated residuals, and those with absolute values larger than 3 have been highlighted.

Statistically, the improvement of the fitness has similar degrees in both kriging approaches. This comes in addition to similar trends of the cross-validated residuals, exhibiting large variations around the same predictor sets (depending upon the predictor's quality in the feasible design space, OLS and IRLS often cannot return the same outliers, since the regression plane is computed differently and also levels of quality of the responses varies across the data when IRLS is performed). This behavior is set a priori by the regularization factor λ, encountered on a higher degree in the latter kriging form. Clearly, the quality of the surface is also controlled by the weighting factor θ and smoothness exponent p across the data, which exhibit small variation of the same vector to the counterpart (see Tables 1–3), augmenting the similarity of the qualities of the two surrogates.

Overall, both kriging definitions exhibit a high degree of accuracy (i.e., correlation). This comes in conjunction with the design-space exploration†† under a two-stage hybrid search of the hyperparameters (i.e., 3000 GA generations with a population size of 100 members used to locate maxima, followed by 2000 DHC evaluations). The performance of the underlying models is also augmented by the convergence rates of the concentrated likelihood function (CLF). The results from the optimized hyperparameters are shown in Tables 4 and 5 as a result of low convergence rates of the hyperparameters from Tables 1 and 2. These results indicate that the problem posed is highly modal [42] or presents long ridges, i.e., within the same bounds of the parameters, the sequential rates of the convergence of the CLF functional for full kriging spans a wider range than for the reduced kriging. Nevertheless, the rate of sequential convergence of full-kriging computation is approximately two times that of the reduced-kriging definition. Although the exploration of the design space is performed on a larger scale in the first case, a similar performance is achieved by the latter kriging. These issues (i.e., multimodality and long ridges) are also augmented by the optimization results for the second constraint from Table 5; the local optimum found with DHC corresponds to the global solution found by the GA after a few iterations, indicating that the optimizer has become stuck in a peak caused by long ridges and may cause a premature convergence.

A set of guidelines on scales of magnitudes of the correlations is suggested by [43], e.g., the correlation of 0.5 is large, 0.3 is medium, and 0.1 is small effect. The last reference subjectively set some conventions of the medium effect, which should have a day-to-day natural consequence and be visible to people, whereas the small effect is noticeably smaller but not trivial, and the large effect should be the same distance above the medium effect as small was below it. Under these conventions, the correlations for all the objectives and constraints in both RSMs approaches can be regarded as large, considering the noise produced by the MDO process for such a large metamodel (the transonic flow conditions have a large impact on the data, as the shocks are very difficult to capture in the trend of the true function). The correlations are also dependent upon the kriging regularization coefficient λ, which indicates very small regression needed for the third objective with full RSM (see Table 1) and for the objectives 2, 3, and 4 in case of the reduced kriging (see Table 3). Intuitively, all these issues conclude that the latter form of kriging is more robust and efficient in terms of model fit and computational expense,‡‡ speeding up the convergence of the combined GA and DHC hybrid search and certainly good enough to predict with.

V. Pareto Framework

Practical engineering problems often have multiple and conflicting design objectives that are accompanied by a large number of design variables. Such problems usually present multiple optimum

††As a reminder, the full formulation of kriging comprises 3 hyperparameters and 19 parameters in the deterministic space; therefore, there are 39 surrogate variables. In the reduced form of kriging, there are three hyperparameters, but the smoothness factor p and weight θ have a global definition; therefore, there are three variables, including regression factor λ.

‡‡Each full-kriging computation with a training pool of 200 DOE LPτ points took around 75 CPU minutes, whereas each reduced definition took around 45 CPU minutes, on a dual-Xeon 2800+ 2 MB machine.

Table 1 Full-kriging definition verification results: hyperparameters for objectives 1–3

f_1		$f_{\text{sec}\,1}$		$f_{\text{sec}\,2}$	
θ	p_h	θ	p_h	θ	p_h
−1.126745	1.999493	−1.985511	1.999245	−0.799206	1.299058
−1.020435	1.550526	−0.396232	1.894310	−0.999121	1.774789
−1.077945	1.971779	−1.178687	1.058657	−7.500733	2.000000
−1.026845	1.995278	−1.005856	1.991235	−1.107923	1.553443
−1.895812	1.997037	−0.688395	1.996956	−0.796045	1.882988
−1.586783	1.997763	−0.992657	1.258804	−1.315167	1.995489
−1.828593	1.000424	−1.141495	1.993417	−1.050012	1.976291
−1.106156	1.962829	−8.521177	1.999328	−0.999206	1.005263
−1.654563	1.995372	−0.694044	1.006119	−7.475312	1.876740
−8.431797	1.046389	−1.949714	1.996709	−0.999219	2.000000
−2.073760	1.998464	−7.680837	1.357814	−2.415972	1.999084
−1.410145	1.771142	−0.799406	1.417534	−1.002381	1.723454
−1.271454	1.000774	−7.069457	1.091782	−0.999246	1.039807
−1.685267	1.952643	−0.850330	1.712001	−0.999256	1.892458
−1.335131	1.996632	−0.856359	1.482013	−0.999206	1.166722
−1.065564	1.996053	−0.802321	1.952058	−0.986529	1.764776
−1.355693	1.667168	−1.008450	1.992362	−0.697693	2.000000
−8.326637	1.064976	−2.052717	1.999210	−0.973845	1.995473
−5.363671	1.927934	−8.302111	1.140232	−0.589354	1.952131
$\lambda = -0.609419$		$\lambda = -13.752930$		$\lambda = -19.695300$	

Table 2 Full-kriging definition verification results: hyperparameters for objective 4 and constraints

$f_{\text{sec}\,3}$		g_1		g_2	
θ	p_h	θ	p_h	θ	p_h
−1.005556	1.996154	−0.999206	1.999817	−1.343734	1.997718
−1.037302	1.997412	−1.002381	1.414301	−7.775972	1.075082
−0.924516	1.793559	−0.999206	1.657922	−1.766182	1.996164
−7.910218	1.325340	−0.999276	1.999322	−1.404127	1.240535
−1.814881	1.996516	−0.973809	1.683150	−1.398357	1.997962
−7.500783	1.523354	−0.999206	1.471723	−1.552874	1.712149
−0.999206	1.004034	−1.715446	1.098821	−1.800244	1.205345
−0.961781	1.057822	−0.986507	1.841967	−1.605525	1.949767
−8.518303	1.968071	−1.549286	1.991824	−1.783214	1.998378
−0.999160	1.740126	−0.999206	1.171978	−9.705468	1.012842
−0.935739	1.740174	−1.242025	1.437657	−1.005943	1.994817
−0.973785	1.997635	−0.999226	1.574973	−2.172607	1.997168
−7.361111	1.303602	−1.811933	1.999497	−7.542584	1.078315
−1.008748	1.995854	−0.999206	1.649594	−1.723414	1.722117
−0.453134	1.562576	−0.999206	2.000000	−0.918343	1.999323
−0.275421	1.872334	−0.999206	2.000000	−0.968278	1.994823
−0.646856	1.800200	−0.853167	1.334120	−1.285786	1.659906
−7.284923	1.057934	−0.973809	1.979283	−1.431930	1.995035
−7.907112	1.031807	−0.897620	1.126834	−0.403639	1.998033
$\lambda = -11.270390$		$\lambda = -18.493350$		$\lambda = -0.448961$	

solutions that may be encapsulated by Pareto-optimality criteria [44]. Each Pareto solution contains a set of data that are optimum in the sense that any improvement toward one objective would worsen another. This interaction between conflicting goals is based on the nondominance concept with respect to the performance criteria. Traditionally, such problems are tackled in a weighted fashion, where multiple objectives are combined into a single goal. Such an approach runs the risk of limiting the conflicting feature of the design sets and is therefore limited in searching for global optimum. This drawback is overcome by another class of algorithms, based on globally nondominated design sets, which comprise the frontier of

Table 4 Full-kriging definition verification results: CLF convergence

	Start	GA	DHC
f_1	800.94275	816.222454	834.993491
$f_{\text{sec}\,1}$	1006.91110	1029.803575	1049.705342
$f_{\text{sec}\,2}$	684.699782	707.606842	731.491481
$f_{\text{sec}\,3}$	208.567645	252.455762	268.567848
g_1	778.307956	793.609048	802.6770674
g_2	111.787458	126.929045	137.855734

Table 5 Hybrid kriging definition verification results: CLF convergence

	Start	GA	DHC
f_1	800.942444	811.709456	816.852962
$f_{\text{sec}\,1}$	1006.911065	1016.636724	1023.85954
$f_{\text{sec}\,2}$	684.699743	699.455330	708.469816
$f_{\text{sec}\,3}$	208.567691	214.996557	215.042456
g_1	778.307861	792.140847	798.252239
g_2	111.787838	123.222285	123.222285

best tradeoff between competing designs. These problems are well tackled by population-based algorithms, e.g., genetic algorithms, which offer diversity in manipulating solutions. A number of approaches in the literature are related to the measure of nondominance; e.g., in [45] the multi-objective GA ranks each individual according to the number of dominated solutions (rank one contains the individuals on the Pareto front); NSGA-II (nondominated sorted genetic algorithm) proposed in [46] is based on a crowding-comparison operator as part of the elitism scheme that attempts to produce a uniformly distributed Pareto front.

In addition to encountering multiple conflicting objectives, engineering problems are also often expensive to search. Depending on the design space and the accuracy required, these problems can be tackled using hybrid formulations of nondominated solutions by means of approximation models combined with genetic operators [17]. In this study, the NSGA-II approach is used to search the parametric space built on preexisting kriging to find the best combinations of the design variables that can minimize the approximated functionals proposed in Eqs. (1–6). The approximation surfaces are based on sampled points from the true function. This constrained search (note that a Fiacco–McCormick penalty function is used [47]) is based on a population size of 100 for 3000 generations and leads to Pareto sets of approximated designs, for both kriging definitions, as shown in Figs. 10 and 11, accompanied by the rank one DOE LPτ design points from both training and predictions data sets. The approximated solutions from the Pareto fronts are then evaluated on the true function by calling the expensive analysis codes, to quantitatively and qualitatively check the surface-based solutions. Since all the Pareto fronts are weak in the constitutive approximated objective space, all the points are checked with the verification scheme (i.e., SWF). This process is limited somewhat due to solver failures (i.e., structural divergence or computational issues) in the design process. The placing of the validated points (taking the Pareto-front definition as a valid basis) is inconclusive at this stage with regard to the prediction quality of the metamodels, although, locally, the currently known Pareto front is close to the approximated one, on which the verification was performed. It should be noted that the Pareto front from the reduced definition underperforms within the same training

Table 3 Hybrid kriging definition verification results: hyperparameters for objectives and constraints

	f_1	$f_{\text{sec}\,1}$	$f_{\text{sec}\,2}$	$f_{\text{sec}\,3}$	g_1	g_2
θ	−1.3696344	−1.23694	−1.261031	−1.060941	−1.285733	−1.056367
p_h	1.996244	1.993633	1.994083	1.658179	1.995557	1.875044
λ	−0.580239	−0.770451	−0.726343	−7.04856	−0.661667	−15.70184

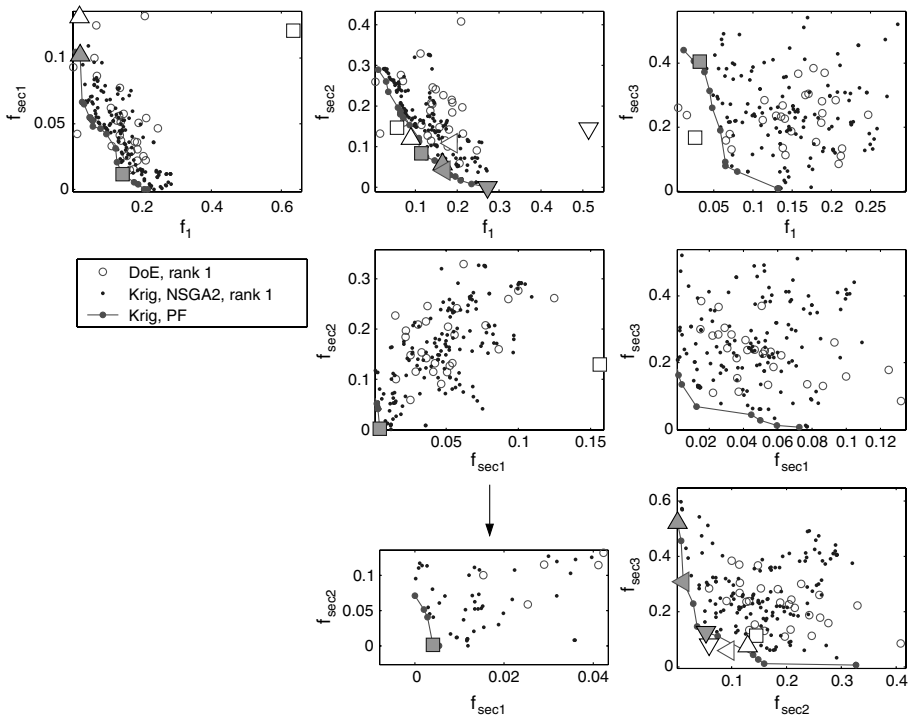

Fig. 10 Full-kriging definition, NSGA2 search, Pareto fronts. Filled symbols represent the solvable points from local Pareto front with the true function. Empty symbols are the corresponding points evaluated with the true function. Some of the filled symbols (solutions) may not perform on the other Pareto fronts, due to failed structural or aerodynamic analyses.

pool of data sets and prediction, taking the nondominated solutions from DOE as a valid basis for comparison (see Fig. 11). Although an exhaustive search on the hyperparameters indicated that the reduced form is robust with good verification metrics, the quality of the surface may suffer in approximating a multimodal function (note that the constitutive hyperparameters clearly affect the shape of the surface through p and θ and thus the quality). These issues lead to the need for an update strategy to be involved, as shown in Fig. 4, until some form of convergence is met (e.g., minimizing the residuals between the approximated and the true function Pareto fronts).

Returning to the initial scope of this section (namely, to analyze the roll enhancement of the underlying model), the best validated points from the Pareto fronts from full kriging involving the first objective are analyzed. The choice of the first objective is strongly emphasized by its definition and scope, which is to provide a direct metric of the aerodynamic properties of the morphed wing.

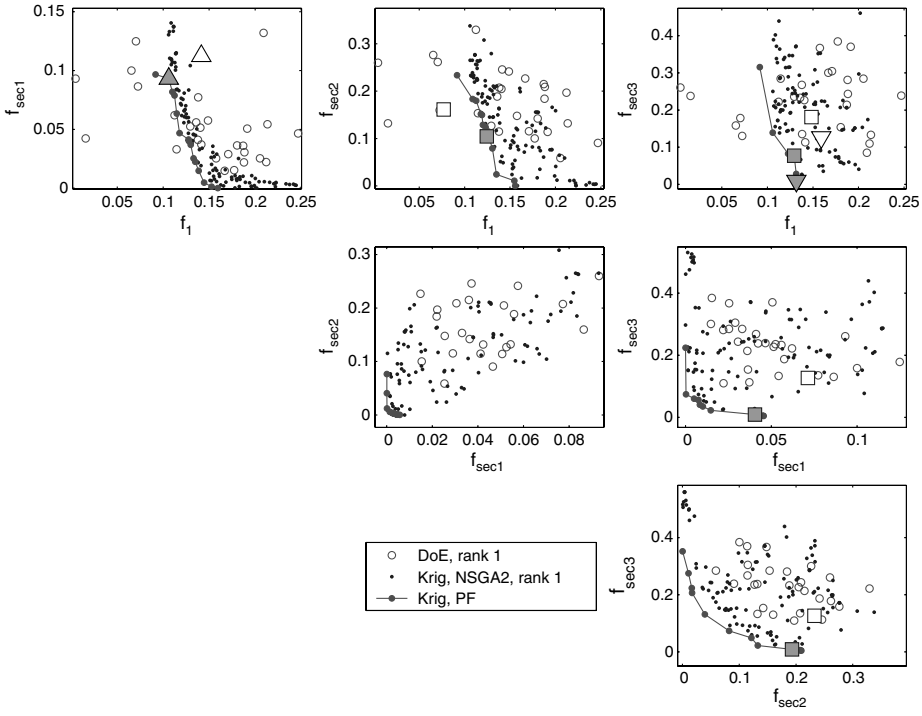

Fig. 11 Reduced kriging definition, NSGA2 search, Pareto fronts. Filled symbols represent the solvable points from local Pareto front with the true function. Empty symbols are the corresponding points evaluated with the true function. Some of the filled symbols (solutions) may not perform on the other Pareto fronts, due to failed structural or aerodynamic analyses.

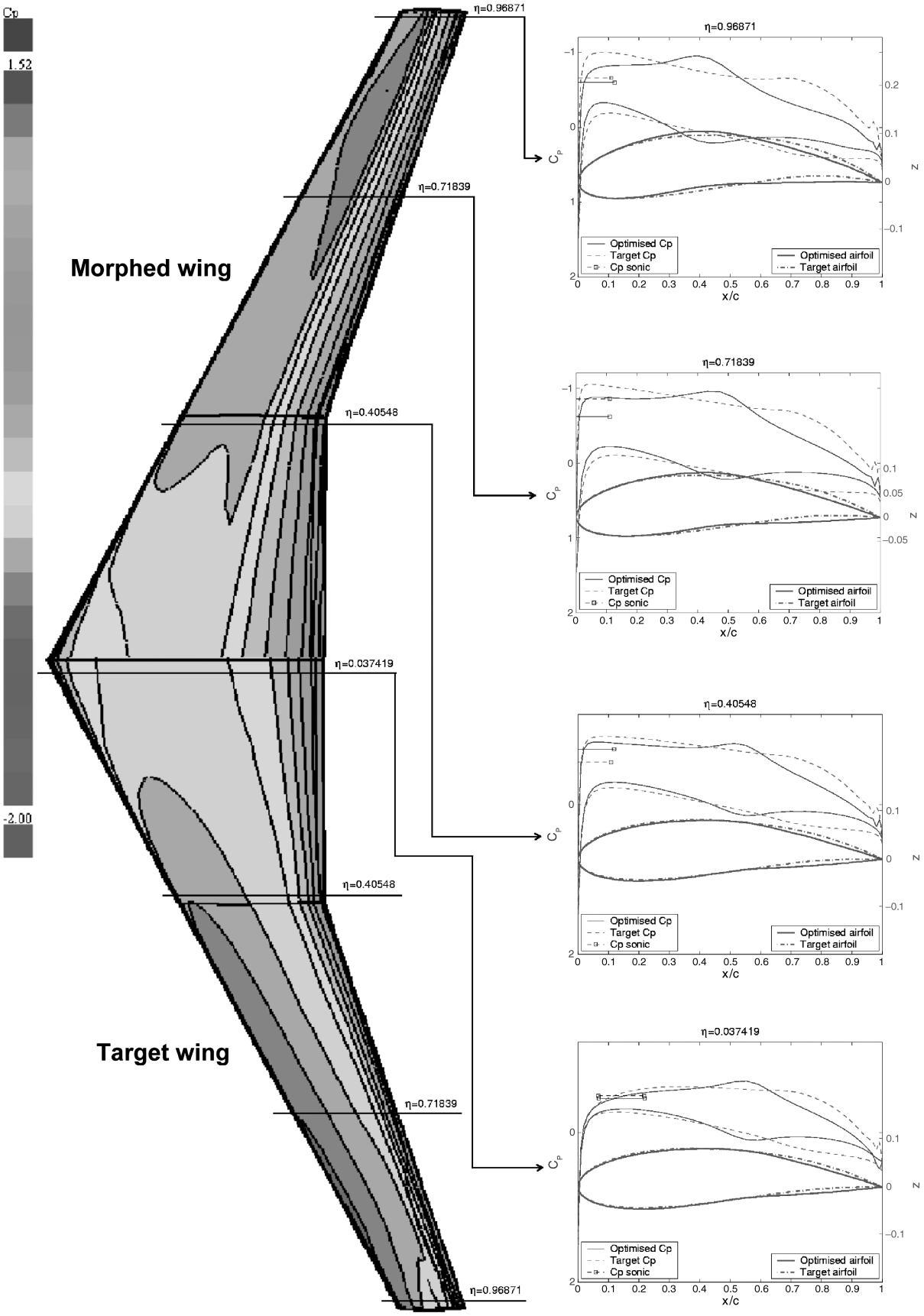

Fig. 12 Pressure contours of a design-validated point (full kriging) from Pareto front $f_1 - f_{\text{sec}\,1}$.

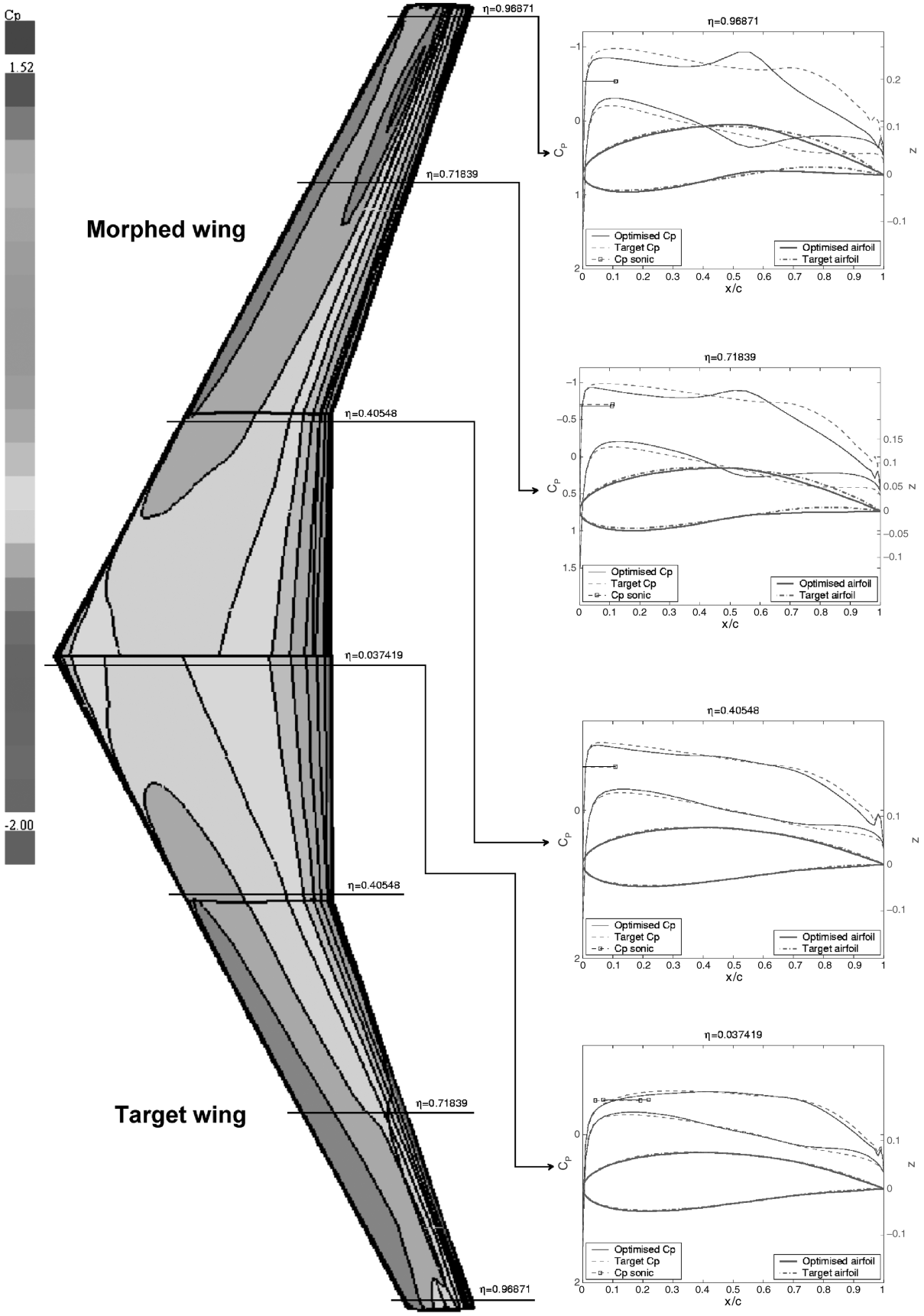

Fig. 13 Pressure contours of a design-validated point (full kriging) from Pareto front $f_1 - f_{\mathrm{sec}\,2}$.

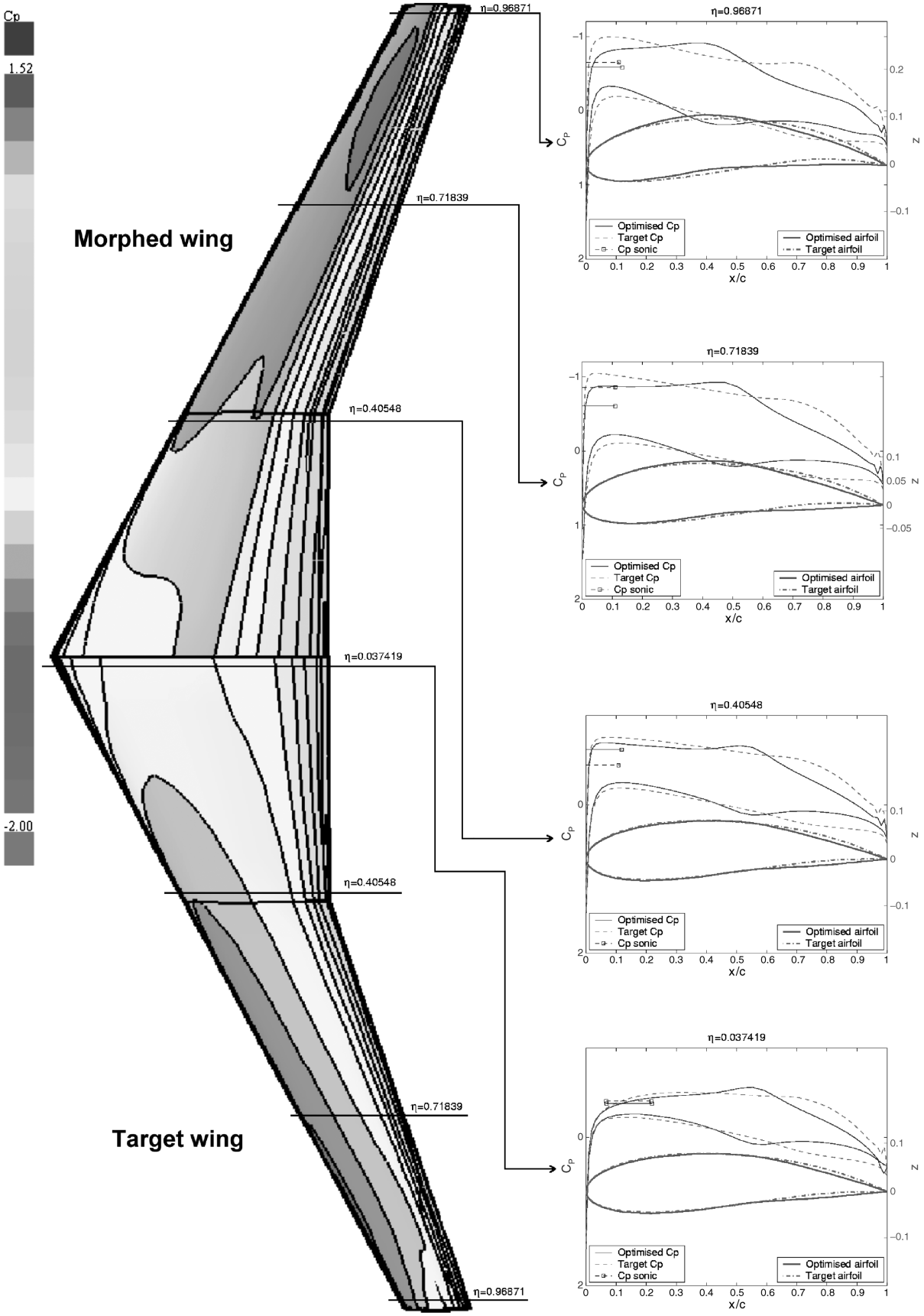

Fig. 14 Pressure contours of a design-validated point (full kriging) from Pareto front $f_1 - f_{\text{sec}\,3}$.

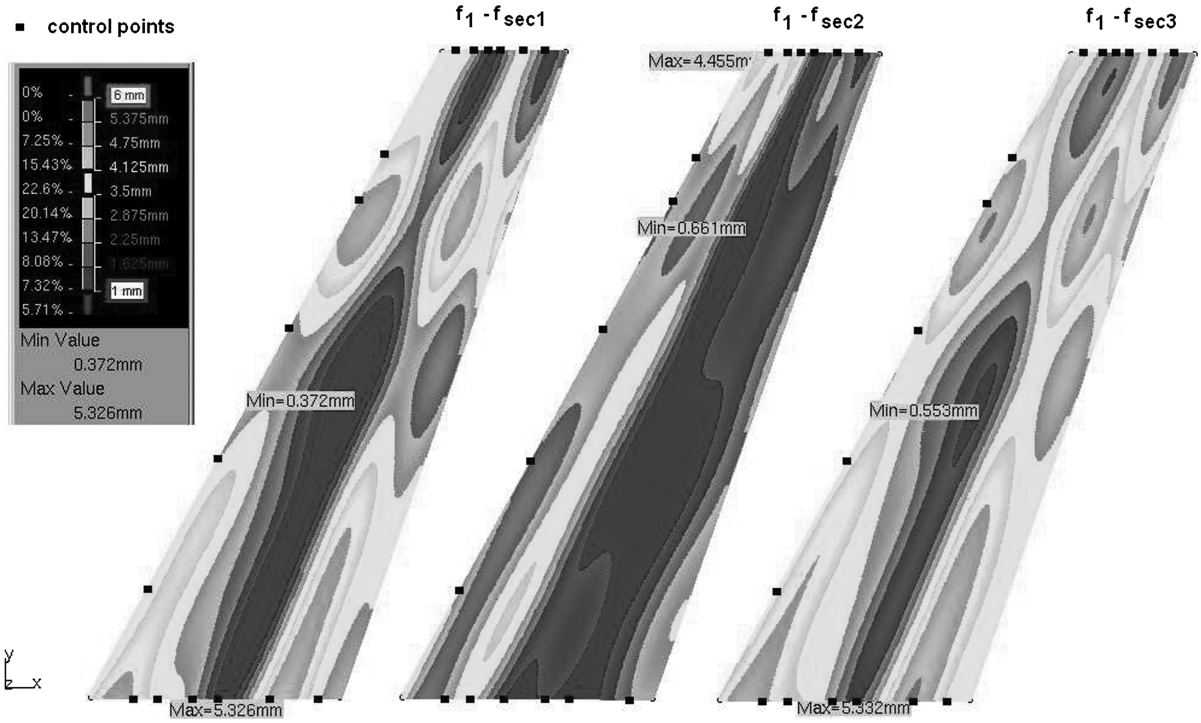

Fig. 15 Camber contours for the design-validated points (full kriging) from Pareto fronts $f_1 - f_{\text{sec}\,1}$, $f_1 - f_{\text{sec}\,2}$, and $f_1 - f_{\text{sec}\,3}$.

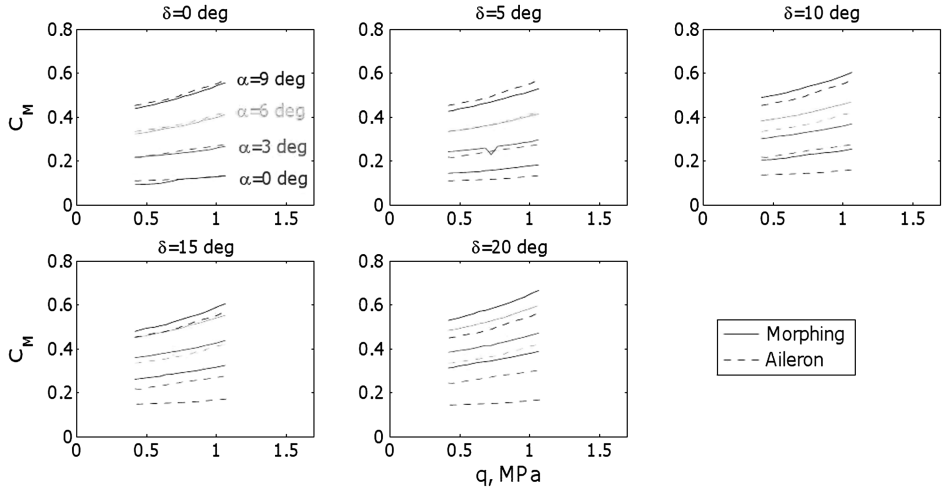

Fig. 16 Roll enhancement of a design-validated point (full kriging) from Pareto front $f_1 - f_{\text{sec}\,1}$.

The resulting designs in terms of pressure contours are presented in Figs. 12–14, and the equivalent camber contours for these design points are shown in Fig. 15. All the designs show pressure distributions somewhat similar to flapped airfoils, due to the curvature changes in the spinal structure. Larger cambers at sections toward the tip of the wing tend to shift the suction peaks toward midchord and lead to larger residuals with respect to the structural and aerodynamic shapes. The morphed airfoils tend to have a two-part form of pressure distribution over the rear, i.e., a low-severity adverse pressure gradient as the trailing edge is approached, followed at $\xi \simeq 0.99$ by a small suction peaks that indicates a sudden boundary-layer separation.

VI. Roll Enhancement

These designs may offer a valid basis for comparison with a wing with conventional control surfaces (25% flap-to-wing-chord ratio), under similar planform parameters in order to provide a roll performance metric as a measure of the morphing wing effectiveness (note that the roll here is provided by a wing when the tip is deflected in the positive direction only and the roll for the whole aircraft can be obtained by a differential positive deflection of the tips of the wings). A standard setup comprising aileron deflection, Mach number, and angle of attack has been built for the conventional and morphing wings.[§§] This covers aileron deployment δ in the range of 0–20 deg, Mach numbers between 0.4 and 0.8 and angles of attack between 0 and 10 deg. The points under investigation represent the best achieved verified solutions in terms of objective f_1 from the Pareto fronts $f_1 - f_{\text{sec}\,1}$, $f_1 - f_{\text{sec}\,2}$, and $f_1 - f_{\text{sec}\,3}$. The results in terms of roll moment coefficient and dynamic pressure are depicted in Figs. 16–18. For aileron deployment up to 5 deg, the morphing wing is underperformed by its counterpart. This is mainly due low induced-twist spanwise distribution and the weak performance of the NACA aft-camber airfoil. Further increasing the deployment, the differences gradually diminish and the morphing roll becomes more

[§§]A range of Mach numbers are verified for the aerodynamic performance of a morphing structure optimized for Mach = 0.78.

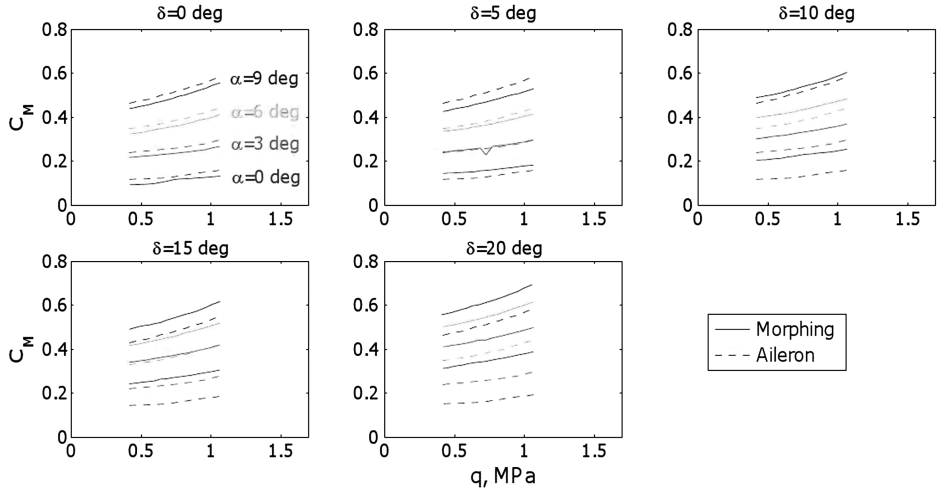

Fig. 17 Roll enhancement of a design-validated point (full kriging) from Pareto front $f_1 - f_{\text{sec}\,2}$.

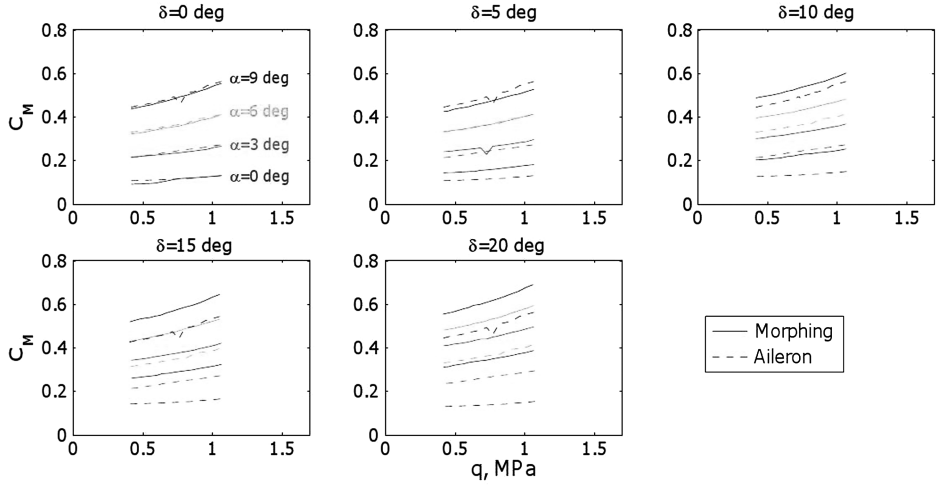

Fig. 18 Roll enhancement of a design-validated point (full kriging) from Pareto front $f_1 - f_{\text{sec}\,3}$.

prominent and outperforms the classical wing to approximately 5% for a 10 deg aileron deployment and 20% for a 20 deg aileron deployment. An immediate benefit of the morphing wing is the continuous control surface, as opposed to the classical wing hingeline discontinuities. For larger aileron deflections, a good performance of the morphing wing at these design points is somewhat expected and is significantly influenced by several factors. For instance, the small tip camber deflection to 4% (exhibited by the design point from the Pareto front $f_1 - f_{\text{sec}\,3}$), twist of approximately 4 deg (flight shape) and constant thickness distribution spanwise. Since the structural deflection is linked to the loading function, the stopping criterion runs the risk of limiting the search on the point forces that produce the controlled bounds of the displacement field, and thus the loading solution becomes nonunique. The performance is also determined by the accuracy of the metamodels built in the initial design stage, where the correlation factor for the objectives vary between 0.51 and 0.81. Clearly, these results give confidence that further updates and refinement of the approximation surfaces will drive the performance improvement by means of stiffness tailoring.

VII. Conclusions

This research paper described a heuristic methodology for designing wings with global shape control. Extending the approach for multishape morphing airfoils into the spanwise direction and based on a simple loading scheme, the morphing wing concept is applied to provide enhanced roll control. The aerodynamic wing design is tackled in a hierarchical multi-objective optimization by means of approximation models combined with NSGA-II to search the Pareto-front framework. The global approximation of the spinal structure provides a means of aerodynamic shape control enhanced by prescribed structural shapes to maintain product integrity by enabling the control surface to smoothly blend the grid-controlled sections and avoid spurious designs.

The complexity of the problem requires a careful examination of the cost functions and the surrogate modeling involved; therefore, it drives the design intent into approaching different definitions of kriging-based response surfaces. To provide acceptable means of compliance, full and hybrid versions of kriging surrogates are studied in order to provide the opportunity to fully correlate the convergence rates. Although both surrogates exhibited a high degree of accuracy, the reduced kriging showed a better robustness and efficiency in terms of model fitness and computational expense.

Overall, the morphing capabilities show good roll control when compared with a classical wing with 20 deg aileron deployment, but the performance of the wing is strictly driven by the choice of structural metrics and constraints. This translates into the need to fully define the target wing shape (by means of blended airfoils) to ensure a particular flowfield that drives the robustness of the inverse design paradigm.

Acknowledgment

This research was supported by a grant from the Faculty of Engineering, Science and Mathematics at the University of Southampton, United Kingdom.

References

[1] Roth, B. D., and Crossley, W. A., "Application of Optimization Techniques in the Conceptual Design of Morphing Aircraft," 3rd AIAA Annual Aviation Technology, Integration and Operations (ATIO) Conf., AIAA Paper 2003-6733, Denver, CO, 17–19 Nov. 2003.

[2] Gilyard, G., Georgie, J., and Barnicki, J. S., "Flight Test of an Adaptive Configuration Optimization System for Transport Aircraft," NASA Dryden Flight Research Center, TM-1999-206569, Edwards AFB, CA, Jan. 1999.

[3] Ursache, N., Bressloff, N., and Keane, A. J., "Design of Postbuckled Spinal Structures for Airfoil Camber and Shape Control," *AIAA Journal*, Vol. 44, No. 12, 2006, pp. 3115–3124. doi:10.2514/1.22636

[4] Austin, F., Rossi, M. J., Nostrand, W. V., Knowles, G., and Jameson, A., "Static Shape Control for Adaptive Wings," *AIAA Journal*, Vol. 32, No. 9, Sept. 1994, pp. 1895–1901. doi:10.2514/3.12189

[5] Seifert, A., Eliahu, S., Greenblatt, D., and Wygnanski, I., "Use of Piezoelectric Actuators for Airfoil Separation Control," *AIAA Journal*, Vol. 36, No. 8, 1998, pp. 1535–1537. doi:10.2514/2.549

[6] Pinkerton, J. L., and Moses, R. W., "A Feasibility Study to Control Airfoil Shape Using Thunder," NASA Langley Research Center, TM-4767, Hampton, VA, Nov. 1997.

[7] Norris, G., "Laminar Flow Control—Smooth and Supersonic," *Flight International*, Vol. 145, No. 4421, May 1994, pp. 32–33.

[8] Scherer, L. B., Martin, C. A., Appa, K., Kudva, J. N., and West, M. N., "Smart Wing Test Results," *Proceedings of SPIE*, Vol. 3044, No. 56, 1997. doi:10.1117/12.274694

[9] Voracek, D., Pendleton, E., Reichenbach, E., Griffin, K., and Welch, L., "The Active Aeroelastic Wing Phase I Flight Research Through January 2003," NASA Dryden Flight Research Center, TM-2003-210741, Edwards AFB, CA, 2003.

[10] Love, M. H., Zink, P. S., Stroud, R. L., Bye, D. R., and Chase, C., "Impact of Actuation Concepts on Morphing Aircraft Structures," 5th AIAA/ASME/ASCE/AHS/ASC Structures, Structural Dynamics & Materials Conf., AIAA Paper 2004-1724, Palm Springs, CA, April 2004.

[11] Mattioni, F., Gatto, A., Weaver, P. M., Friswell, M. I., and Potter, K. D., "The Application of Residual Stress Tailoring of Snap-Through Composites for Variable Sweep Wings," 47th AIAA/ASME/ASCE/AHS/ASC Structures, Structural Dynamics, and Materials Conf., AIAA Paper 2006-1972, Newport, RI, 2006.

[12] Herencia, J. E., Weaver, P. M., and Friswell, M. I., "Optimization of Long Anisotropic Laminated Fiber Composite Panels with T-shaped Stiffeners," *AIAA Journal*, Vol. 45, No. 10, 2007, pp. 2497–2509. doi:10.2514/1.26321

[13] Bourdin, P., Gatto, A., Friswell, M. I., and Potter, K. D., "The Application of Variable Cant Angle Winglets for Morphing Aircraft Control," 24th Applied Aerodynamics Conf., AIAA Paper 2006-3660, San Francisco, 5–8 June 2006.

[14] Ursache, N., Melin, T., Isikveren, A. T., and Friswell, M., "Morphing Winglets for Aircraft Multiphase Improvement," 7th AIAA Aviation Technology, Integration and Operations Conf. (ATIO), AIAA Paper 2007-7813, Belfast, Northern Ireland, 18–20 Sept. 2007.

[15] McGowan, A.-M. R., Washburn, A. E., Horta, L. G., Bryant, R. G., Robert, Cox, D. E., Siochi, E. J., Padula, S. L., and Holloway, N. M., "Recent Results from NASA's Morphing Project," *Proceedings of SPIE*, Vol. 4698, 2002, pp. 97–111. doi:10.1117/12.475056.

[16] Matthies, H., and Strang, G., "The Solution of Nonlinear Finite Element Equations," *International Journal for Numerical Methods in Engineering*, Vol. 14, 1979, pp. 1613–1626. doi:10.1002/nme.1620141104

[17] Keane, A. J., and Nair, P. B., *Computational Methods for Aerospace Design: The Pursuit of Excellence*, Wiley, Chichester, England, U.K., 2005.

[18] Maskew, B., "Program VSAERO Theory Document. A Computer Program for Calculating Nonlinear Aerodynamic Characteristics of Arbitrary Configurations," NASA, CR 4023, Sept. 1987.

[19] Jameson, A., and Vassberg, J. C., "Computational Fluid Dynamics for Aerodynamic Design: Its Current and Future Impact," 39th AIAA Aerospace Sciences Meeting & Exhibit, AIAA Paper 2001-0538, Jan. 2001.

[20] Samareh, J. A., "Shape Parameterization Techniques for High-Fidelity Multidisciplinary Shape Optimization," *AIAA Journal*, Vol. 39, No. 5, 2001, pp. 877–883. doi:10.2514/2.1391

[21] Piegl, L., and Tiller, W., *The NURBS Book*, 2nd ed., Springer–Verlag, Berlin, Jan. 1997.

[22] Smith, B., Rinaudot, G., Reed, K., and Wright, T., "The Initial Graphics Exchange Specification (IGES Version 4.0)," National Bureau of Standards, NBRSIR 88-3813, Gaithersburg, MD, June 1988.

[23] Crisfield, M. A., *Non-Linear Finite Element Analysis of Solids and Structures*, Vol. 1, Wiley, Chichester, England, U.K., 1997.

[24] Riks, E., "An Incremental Approach to the Solution of Snapping and Buckling Problems," *International Journal of Solids and Structures*, Vol. 15, 1979, pp. 529–551. doi:10.1016/0020-7683(79)90081-7

[25] Steen, E., "Application of the Perturbation Method to Plate Buckling Problems," Mechanics Div., Department of Mathematics, Univ. of Oslo, Rept. 98-1, Oslo, Norway, 1998.

[26] Koiter, W. T., "Some Properties of Completely Symmetric Multilinear Forms with an Application to Ho's Theorem for Multi-mode Buckling," Delft Univ. of Technology, Delft, The Netherlands, 1976.

[27] Lovejoy, A. E., and Kapania, R. K., "Static and Vibration Analyses of General Wing Structures using Equivalent-Plate Models," Center for Composite Materials and Structures, Virginia Polytechnic Inst. and State Univ., Rept. CCMS-94-09, Blacksburg, VA, Aug. 1994.

[28] Von Kármán, T., "Festigkeitsprobleme in Maschienbau," *Encyklopädie der Matematischen Wissenschafen*, Vol. 4, 1970, Chap. 27, p. 349.

[29] Dawe, D. J., "Buckling and Vibration of Plate Structures Including Shear Deformation and Related Effects," *Aspects of the Analysis of Plate Structures*, edited by D. J. Dawe, R. W. Horsington, A. G. Kamtekar, and G. H. Little, Oxford Univ. Press, New York, 1985.

[30] Mindlin, R. D., "Influence of Rotatory Inertia and Shear on Flexural Motions of Isotropic Elastic Plates," *Journal of Applied Mechanics*, Vol. 18, 1951, pp. 31–38.

[31] Hughes, T. J. R., Taylor, R. L., and Kanoknukulchai, W., "A Simple and Efficient Finite Element for Plate Bending," *International Journal for Numerical Methods in Engineering*, Vol. 11, No. 10, 1977, pp. 1529–1543. doi:10.1002/nme.1620111005

[32] Wong, Y. W., and Pellegrino, S., "Computation of Wrinkle Amplitudes in Thin Membranes," 43rd AIAA/ASME/ASCE/AHS/ASC Structures, Structural Dynamics, and Materials Conf., AIAA Paper 2002-1369, Denver, CO, 22–25 April 2002.

[33] Mead, R., *The Design of Experiments*, Cambridge Univ. Press, Cambridge, England, U.K., 1998.

[34] Holland, J. H., *Adaptation in Natural and Artificial Systems: An Introductory Analysis with Applications to Biology, Control and Artificial Intelligence*, MIT Press, Cambridge, MA, 1992.

[35] Yuret, D., and de la Maza, M., "Dynamic Hill Climbing: Overcoming the Limitations of Optimization Techniques," *Proceedings of the 2nd Turkish Symposium on AI and ANNI*, 1993.

[36] Simpson, T. W., Mauery, T. M., Korte, J. J., and Mistree, F., "Kriging Models for Global Approximation in Simulation-Based Multidisciplinary Design Optimization," *AIAA Journal*, Vol. 39, No. 12, Dec. 2001, pp. 2233–2241. doi:10.2514/2.1234

[37] DuMouchel, W. H., and O'Brien, F. L., "Integrating a Robust Option into a Multiple Regression Computing Environment," *Computer Science and Statistics: Proceedings of the 21st Symposium on the Interface*, 1989.

[38] Myers, R. H., and Montgomery, D. C., *Response Surface Methodology: Process and Product Optimization Using Designed Experiments*, Wiley, New York, 1995.

[39] Rousseuw, P. J., and Leroy, A. M., *Robust Regression and Outlier Detection*, Wiley, New York, 1987.

[40] Kim, H., "Statistical Modeling of Simulation Errors and Their Reduction via Response Surface Techniques," Ph.D. Thesis, Virginia Polytechnic Inst. and State Univ., Blacksburg, VA, June 2001.

[41] Wager, T. D., Keller, M. C., Lacey, S. C., and Jonides, J., "Increased Sensitivity in Neuroimaging Analyses Using Robust Regression," *Neuroimage*, Vol. 26, 2005, pp. 99–113. doi:10.1016/j.neuroimage.2005.01.011

[42] Warnes, J. J., and Ripley, B. D., "Problems with Likelihood Estimation of Covariance Function of Spatial Gaussian Processes," *Biometrika*, Vol. 74, No. 3, 1987, pp. 640–642. doi:10.1093/biomet/74.3.640

[43] Cohen, J., "A Power Primer," *Psychological Bulletin*, Vol. 112, 1992, pp. 155–159. doi:10.1037/0033-2909.112.1.155

[44] Miettinen, K. M., *Nonlinear Multiobjective Optimization*, Kluwer, Boston, 1999.

[45] Fonseca, C. M., and Fleming, P. J., "Genetic Algorithms for Multiobjective Optimization: Formulation, Discussion and Generalization," *Proceedings of the 5th International Conference on Genetic Algorithms*, Vols. 849–858, Morgan Kaufmann, San Francisco, 1993.

[46] Deb, K., Agrawal, S., Pratap, A., and Meyarivan, T., "A Fast Elitist Non-Dominated Sorting Genetic Algorithm for Multi-Objective Optimization: NSGA-II," *PPSN VI Proceedings of the 6th International Conference on Parallel Problem Solving from Nature*, Vol. 1917, Springer–Verlag, London, 2000, pp. 849–858.

[47] Fiacco, A. V., and McCormick, G. P., *Nonlinear Programming: Sequential Unconstrained Minimization Techniques*, Wiley, New York, 1968.

T. Zang
Associate Editor